An Exhaustive Multiple Knockout Approach to Understanding Cell Wall Hydrolase Function in *Bacillus subtilis*

Sean Wilson[1,2], Ethan Garner[1,2,*]

[1] Department of Molecular and Cellular Biology, Harvard University, Cambridge, United States.

[2] Center for Systems Biology, Harvard University, Cambridge, United States.

Corresponding Author: Ethan C. Garner

NW 445.20, Northwest Building, 52 Oxford Street, Cambridge, MA 02138

*E-mail: egarner@g.harvard.edu

ABSTRACT

Most bacteria are surrounded by their cell wall, a highly crosslinked protective envelope of peptidoglycan. To grow, bacteria must continuously remodel their wall, inserting new material and breaking old bonds. Bond cleavage is performed by cell wall hydrolases, allowing the wall to expand. Understanding the functions of individual hydrolases has been impeded by their redundancy: single knockouts usually present no phenotype. We used an exhaustive multiple-knockout approach to determine the minimal set of hydrolases required for growth in *Bacillus subtilis.* We identified 42 candidate cell wall hydrolases. Strikingly, we were able to remove all but two of these genes in a single strain; this "Δ40" strain shows a normal growth rate, indicating that none of the 40 hydrolases are necessary for cell growth. The Δ40 strain does not shed old cell wall, demonstrating that turnover is not essential for growth.

The remaining two hydrolases in the Δ40 strain are LytE and CwlO, previously shown to be synthetically lethal. Either can be knocked out in Δ40, indicating that either

hydrolase alone is sufficient for cell growth. Environmental screening and zymography revealed that LytE activity is inhibited by Mg^{2+} and that RlpA-like proteins may stimulate LytE activity. Together, these results demonstrate that the only essential function of cell wall hydrolases in *B. subtilis* is to enable cell growth by expanding the wall and that LytE or CwlO alone is sufficient for this function. These experiments introduce the Δ40 strain as a tool to study hydrolase activity and regulation in *B. subtilis*.

IMPORTANCE

In order to grow, bacterial cells must both create and break down their cell wall. The enzymes that are responsible for these processes are the target of some of our best antibiotics. Our understanding of the proteins that break down the wall – cell wall hydrolases – has been limited by redundancy among the large number of hydrolases many bacteria contain. To solve this problem, we identified 42 cell wall hydrolases in *Bacillus subtilis* and created a strain lacking 40 of them. We show that cells can survive using only a single cell wall hydrolase; this means that to understand the growth of *B. subtilis* in standard laboratory conditions, it is only necessary to study a very limited number of proteins, simplifying the problem substantially. We additionally show that the Δ40 strain is a research tool to characterize hydrolases, using it to identify 3 'helper' hydrolases that act in certain stress conditions.

INTRODUCTION

Most bacterial cells are surrounded by a peptidoglycan (PG) cell wall – a load-bearing structure that protects cells from lysing due to their high internal turgor (1). Bonds must be broken in the PG for cells to expand during growth (2). PG is built from disaccharide subunits linked to stem peptides. As new PG is inserted into the wall, the

disaccharides are polymerized into long chains, and their stem peptides are crosslinked into the existing wall (3).

The enzymes that break PG bonds are termed cell wall hydrolases (hereafter 'hydrolases'). Hydrolases fall into several broad categories with different chemical specificities (4). Amidases cleave the stem peptide from the sugar subunit. Endopeptidases cleave bonds between peptides within the stem peptide. Lytic transglycosylases (LTGs), lysozymes/muramidases, and glucosaminidases cleave between sugar subunits. A wide array of different protein domains are capable of hydrolase activity – for example, there are at least 7 distinct domains with LTG activity and well over 100 distinct domains with hydrolase activity discovered thus far (5, 6).

Hydrolase activity is essential: without the breakage of PG bonds, the cell wall cannot expand to accommodate the accumulating biomass it contains (2). Hydrolases are also involved in a variety of other processes that require modification of the cell wall: turning over old PG, cell separation, and sporulation, conjugation, and motility (4, 7). Perhaps owing to the multiple cellular functions that require hydrolases, many bacteria have a large number of hydrolases. *Bacillus subtilis* and *Escherichia coli,* for example, each contain at least 20 hydrolases (4, 8). The large number of hydrolases in each bacterium, combined with a high degree of functional and enzymatic redundancy between them, has made it difficult to identify specific cellular functions for many hydrolases. Single knockouts rarely present clear phenotypes due to compensation by other hydrolases (4, 9). However, multiple-knockout approaches in *B. subtilis* have been successful in revealing the importance of LytE and CwlO for cell growth, uncovering the

role of LytC and LytD in cell wall turnover, and identifying LytE, LytF, and CwlS as cell separation hydrolases (4, 10, 11).

lytE and *cwlO* had been previously shown to be synthetically lethal when both are deleted in *B. subtilis* (10, 12). The requirement of LytE or CwlO for cell growth was demonstrated via microscopy: upon depletion of LytE in a *cwlO* null mutant, or vice versa, cell elongation slows and then stops completely before cells lyse (12). To test whether any other hydrolases were essential for *B. subtilis* growth, we employed an exhaustive multiple-knockout approach. We created a minimal hydrolase strain that allows the study of hydrolases in isolation, making it easier to assign functions to uncharacterized hydrolases. Using this multiple hydrolase knockout strain, it is straightforward to assay the biochemical activity and determine the effect of hydrolases alone or in any desired combination on phenotypes like cell width, cell wall turnover, cell growth, or any other process.

RESULTS

Construction of a multiple hydrolase knockout strain

To identify the minimal set of hydrolases required for growth in *B. subtilis* PY79, we constructed a strain in which we sequentially removed as many hydrolases as possible. First, we used PHMMER to screen the *B. subtilis* proteome for proteins homologous to known hydrolases (4, 5, 8, 13, Table S2). We filtered our results to identify candidates for hydrolases involved in growth with the following criteria: candidates needed to: 1. have a functional hydrolase domain, 2. be secreted (enabling access to the cell wall) and 3. be endo-acting, meaning that they can cleave internal bonds rather than acting only on the ends of the stem peptide or glycan chains (exo-

acting) (4, 14), as exo-acting hydrolases, like the D,D-carboxypeptidase DacA or the glucosaminidase NagZ, cannot contribute to cell growth because their activity does not cause PG expansion. Candidates with the potential to be endo-acting were assumed to be endo-acting unless proven otherwise. Candidate hydrolases that fit all above criteria are indicated in Table 1. Cell wall hydrolases not present in PY79, our wild-type (WT) background, are included for completeness.

We next generated single knockouts for each of the candidate hydrolases by replacing the gene with an antibiotic resistance cassette flanked by loxP sites. We then sequentially combined all knockouts into a single strain, using Cre-lox mediated loop outs to remove markers when necessary (Figure 1). After each loop out step, we verified deletion of all modified loci by PCR. After all knockouts had been combined into a single strain, whole-genome sequencing was used to confirm all deletions and to identify any genomic rearrangements or mutations that occurred during the construction process. Despite the multiple rounds of transformation and loop outs this strain was subjected to, we found no evidence of genomic rearrangements, and only 8 SNPs leading to 5 point mutations in genes involved in unrelated processes (Table S1).

Ultimately, this effort produced a strain lacking 40 hydrolases, which we termed "Δ40". The Δ40 strain is lacking all the identified hydrolases that met our criteria save two - LytE and CwlO, two synthetically lethal endopeptidases previously shown to be essential for growth (10). We were able to further knock out either *lytE* or *cwlO* in the Δ40 strain, but not both, due to their synthetic lethality.

Hydrolase activity is greatly reduced in the Δ40 strain

To assess whether any other unidentified hydrolases remained in the Δ40 strain, we first used zymography. Zymography is a renaturing SDS-PAGE assay for that detects hydrolase activity (15), where cells wall binding proteins are extracted from cells and separated by size via SDS-PAGE using a gel impregnated with purified cell walls. Following separation by PAGE, proteins in the gel are renatured, and their activity cleaves the purified cell wall in the gel, leading to clear "bands" in the gel which do not stain with methylene blue, corresponding to the molecular weight of the protein with hydrolase activity. It is important to note that zymography can only report on a subset of hydrolases: hydrolases must successfully refold after denaturation and have *in vitro* activity in the absence of any co-factors. Because either LytE or CwlO must be present for viability, we conducted zymograms on the Δ40, Δ40 Δ*lytE,* and Δ40 Δ*cwlO* strains (Figure 2A). The Δ40 strain showed only a single band of hydrolase activity, and this band disappeared upon deletion of *lytE*. Thus, LytE is the only hydrolase detectable via zymography in the Δ40 strain. We note that, although CwlO is also present in Δ40, we do not expect to detect it by zymography, as previous zymography experiments have suggested that full-length CwlO is inactive *in vitro* (16), an effect likely arising from CwlO's auto-inhibitory coiled-coil domain (17).

To detect the activity of hydrolases not visible via zymography, we conducted PG profiling of both wild type (WT) cells and the Δ40 strain (18), allowing us to determine the abundance of hydrolase products in their cell walls (Figure 2B). During sample preparation for PG profiling, we omitted teichoic acid removal to prevent sample degradation: normally, teichoic acids are removed by treatment with a strong acid (18, 19), but this treatment also caused some hydrolysis of amide bonds in the PG,

complicating our analysis (Figure S1). The omission of the teichoic acid removal step has been previously shown not to affect the results of PG profiling other than the disappearance of phosphate-containing muropeptides, species not included in our analysis (18).

Our PG profiling assay has limitations: as PG profiling relies on muramidase digestion to yield soluble muropeptides for HPLC analysis, we could not use this assay to detect hydrolases with muramidase activity. Likewise, D,D-endopeptidases cannot be detected by PG profiling, as they produce products that are indistinguishable from unmodified PG.

We compared the relative abundance of different PG hydrolase products in the Δ40 and WT strains (Figure 2B). The Δ40 strain showed an absence of amidase activity and a strong reduction of glucosaminidase activity, indicating that these classes of hydrolases had been successfully reduced in the Δ40 strain. The residual glucosaminidase activity could represent A) a yet unknown minor glucosaminidase with a novel fold or B) sample degradation during PG purification. We observed an increase in D,L-endopeptidase activity in the Δ40 strain, an expected result given Δ40 retains the D,L-endopeptidases LytE and CwlO. In agreement with previous work (18), L,D-endopeptidase activity was not detected in any strain.

Unexpectedly, the Δ40 strain also showed an increase in LTG activity (Figure 2B). We found that this remaining LTG activity required SweC, a recently characterized membrane-bound CwlO co-factor homologous to the *E. coli* LTG MltG (20) (Table 1). Removing *sweC* from the Δ40 strain eliminated all detectible LTG activity (Figure 2B). However, as SweC's catalytic PG hydrolase domain is cytoplasmic (21), SweC cannot

target the cell wall directly and thus is unlikely to be the direct cause of the residual LTG activity. *B. subtilis* also contains a second membrane protein homologous to MltG, called YrrL. YrrL's catalytic domain is predicted to be extracellular, although YrrL is likely too small to reach far enough into the cell wall space to directly participate in cell wall expansion. Rather, YrrL may instead be involved in the insertion of new cell wall material, as previously proposed for MltG in *E. coli* (20). If YrrL is indeed the source of the residual LTG activity, its activity must require SweC; perhaps YrrL is activated by interactions with SweC or SweD, similar to what has been seen for CwlO (21).

Cell growth and morphology are similar in the Δ40 strain relative to wild type.

We next characterized the growth rate of the Δ40 strain. The Δ40 strain grew at the same rate as WT cells in both rich (CH) and synthetic media ($S7_{50}$ with glucose and amino acids, see Methods for details) (Figure 3A and B). This indicates that the activity of LytE and CwlO together are sufficient for normal cell growth. To investigate the individual effects of each of these enzymes, we made knockouts of *lytE* and *cwlO* in both WT and Δ40 backgrounds. Δ40 Δ*lytE* and Δ40 Δ*cwlO* both exhibited a ~10% reduction in growth rate compared to Δ40. We observed cell lysis in both Δ40 Δ*lytE* and Δ40 Δ*cwlO* strains in phase-contrast images, which could contribute to their slower growth rates as measured in bulk by OD_{600} (Figure 3D). On the other hand, Δ*lytE* or Δ*cwlO* in a WT background had the same growth rate as WT. This suggests either that in WT cells, other hydrolases participate in but are not required for growth, or that LytE and CwlO are not being expressed highly enough to maintain normal growth on their own in the Δ40 background.

Next, we quantified cell dimensions in these strains using FM 5-95 membrane stain. Δ40 cells had a WT cell length and were 3% wider ($p<0.0001$, unpaired t-test with Welch's correction). Δ*cwlO* cells were 13% wider and 18% shorter than WT cells, a phenotype that persisted in the Δ40 Δ*cwlO* strain ($p<0.0001$ for all comparisons: unpaired t-test with Welch's correction for width comparisons, Mann-Whitney test for length comparisons). Δ40 Δ*cwlO* cells were less able to control their width as compared to Δ40 cells, having a 1.5x wider cell width distribution (7.5% vs. 11.33% coefficient of variation, F test $p<0.001$). In contrast, Δ*lytE* cells were only slightly wider than WT cells (1%, $p<0.0001$, unpaired t-test with Welch's correction), and Δ40 Δ*lytE* cells were slightly narrower (1%, $p<0.0001$, unpaired t-test with Welch's correction) than Δ40 strain alone, with a slight decrease in length (Figure 3C, $p<0.0001$, Mann-Whitney test). Thus, CwlO appears to be involved in cell width maintenance, as removing *cwlO* causes changes in cell width both in Δ40 and WT backgrounds, consistent with previous reports (12). Furthermore, given that removing *cwlO* increases the cell width coefficient of variation in the Δ40 background but does not increase the width variation when deleted from WT cells, other hydrolases must also have a role in width homeostasis.

Δ40 cells do not turn over their cell wall

Hydrolases are involved in cell wall turnover, where old PG material is shed from the cell wall (22). We measured the rate of cell wall turnover of both WT and Δ40 cells using pulse-chase labeling with the radioactive cell wall precursor ^{3}H-N-acetylglucosamine (^{3}H-GlcNAc). This revealed that, while WT cells turn over PG at a rate of about 50% per generation in agreement with previous work (22), turnover in Δ40 strain was absent, with a rate not significantly different from zero ($p=0.4837$) (Figure

3A). These results demonstrate that LytE and CwlO, the only identifiable remaining hydrolases in the Δ40 strain, do not contribute to cell wall turnover. Furthermore, this data reveals that cell wall turnover is not an essential process: cell growth only requires the cleavage of bonds so the cell can expand.

As hydrolases have been shown to be involved in the regulation of cell wall thickness (23), we measured the cell wall thickness of the Δ40 strain by transmission electron microscopy (TEM), finding it was not significantly different from WT ($p=0.1382$) (Figure 3B). This suggests that cell wall turnover has no impact on cell wall thickness and that none of the 40 hydrolases removed in the Δ40 strain are responsible for cell wall thickness regulation. Given previous studies have demonstrated hydrolases regulate cell wall thickness, the unchanged cell wall thickness thicknesses observed in our Δ40 demonstrate that LytE and CwlO are the hydrolases controlling cell wall thickness, as these hydrolases are the only non-integral membrane hydrolases remaining.

Δ40 Δ*cwlO* cells are sensitive to various stresses, including ionic stress

Although the Δ40 strain grows normally under our standard lab conditions, we wondered whether the absence of so many hydrolases would sensitize cells to stress conditions. We used a spot dilution assay to measure the viability of our strains under a variety of stress conditions: temperature, ionic stress, pH, and osmotic pressure (Figure 5). In all conditions, including our control (37˚C), Δ40 cells had fewer CFUs than WT. This is expected because Δ40 cells grow in long chains, and thus cells are cannot readily separate into individual CFUs; we do not believe that this reflects an overall change in viability because Δ40 grows at the same rate as WT (Figure 3). In all stress

conditions Δ40 cells were similarly viable to WT cells, as were Δ*lytE,* Δ*cwlO,* and Δ40 Δ*lytE* cells. However, Δ40 Δ*cwlO* cells were susceptible to multiple stresses, including low pH, low temperature, and ionic stress.

We were particularly intrigued by the susceptibility of Δ40 Δ*cwlO* to Mg^{2+}. Mg^{2+} is coordinated between PG and teichoic acids (24), and this Mg^{2+} binding is thought to give structural stability to the cell wall (25, 26). High levels of Mg^{2+} are often protective against cell wall perturbations, including knockouts of hydrolases, PBPs, or components of the rod complex (10, 27); thus, the Mg^{2+} sensitivity of the Δ40 Δ*cwlO* strain seemed counterintuitive. Our experiments indicated Δ40 Δ*cwlO* cells were sensitive to both Ca^{2+} and Mg^{2+}; growth was inhibited by the addition of 10 mM $MgCl_2$, 10 mM $MgSO_4$, and 10 mM $CaCl_2$, but not by the addition of 20 mM NaCl, suggesting that the growth inhibition was not due to changes in ionic strength or chloride ions. We did observe growth inhibition due to ionic stress at far higher salt concentrations (500 mM NaCl). Notably, cells were not sensitive to an equivalent osmotic stress (1M sorbitol), indicating the sensitivity is to ionic stress, not osmotic.

As Δ*cwlO* mutants in the WT background were Mg^{2+} insensitive, we sought to identify which hydrolases caused cells to be sensitive to Mg^{2+} when they were removed. To find these hydrolases, we returned to intermediate strains used to construct the Δ40 strain, which are missing subsets of hydrolases. We transformed a *cwlO* knockout into these intermediate strains, then screened these crosses for the same small colony phenotype and the Mg^{2+} sensitivity seen in the Δ40 Δ*cwlO* strain. This identified two genes: *yabE* and *ydjM*. Notably, during construction of the Δ40 strain, we had noticed that *yocH* seemed significant – at several intermediate verification steps, a WT copy of

yocH had reintegrated itself. Furthermore, a Δ*ydjM* Δ*yocH* Δ*cwlO* mutant was previously demonstrated to be sick, with short and sometimes anucleate cells (10). Because *yabE*, *ydjM*, and *yocH* have similar hydrolase domains, and because *yocH* and *ydjM* had been identified previously to be involved in a synthetic sick interaction with *cwlO,* we additionally tested whether the removal of *yocH* contributed to the Δ40 Δ*cwlO* Mg^{2+} sensitivity phenotype, and found that it did.

In total, we identified three genes, *yabE*, *ydjM*, and *yocH*, whose absence in a Δ*cwlO* background caused the Mg^{2+} sensitivity: A Δ*yabE* Δ*ydjM* Δ*yocH* Δ*cwlO* strain showed a similar stress profile to Δ40 Δ*cwlO*, including sensitivity to $MgCl_2$ and $CaCl_2$ (Figure 6A). *yabE*, *ydjM*, and *yocH* are 3 uncharacterized RlpA-like superfamily domain-containing proteins expressed during exponential growth. Like *lytE* and *cwlO, yocH* and *ydjM* are in the *walR* regulon, while *yabE* is regulated by *sigA* (Table 1). All are likely lytic transglycosylases: *yocH* has been shown to have lytic activity and has homology to the *E. coli* lytic transglycosylase *mltA* (28), and all three share a similar catalytic domain. Because *yabE*, *ydjM*, and *yocH* all contain a RlpA-like protein domain, we refer to these genes collectively as RLPAs, and to the triple deletion of all three genes as ΔRLPAs.

LytE is inhibited by Mg^{2+} *in vitro* and *in vivo*, and RLPAs suppress Mg^{2+} lethality *in vivo*

Finally, we sought to identify the source of Mg^{2+} growth inhibition in the ΔRLPAs Δ*cwlO* background. Because LytE is essential in the absence of CwlO, we hypothesized that the sensitivity of the Δ40 Δ*cwlO* strain to Mg^{2+} (and, by extension, the sensitivity of the ΔRLPAs Δ*cwlO* strain to Mg^{2+}) could be explained by Mg^{2+} inhibition of LytE. To investigate this, we first characterized the response of Δ*cwlO* cells to the removal of

LytE. We constructed an otherwise wildtype strain with *cwlO* knocked out and *lytE* under inducible control and monitored its growth by time-lapse phase-contrast microscopy. When *lytE* was induced, cell growth was normal (Movie S1). When *lytE* induction was removed, cell growth initially slowed, followed by a period of 'stuttery' growth, where elongating cells intermittently shrank while showing accompanying fluctuations in their phase contrast signal (Movie S2). Ultimately, cells lysed about 1-2 doubling times after the removal of *lytE* induction as previously observed (10, 12). Next, we performed the same imaging in the ΔRLPAs Δ*cwlO* strain after the addition of 10 mM $MgCl_2$ and observed the same 'stuttery' phenotype, suggesting that LytE function might be inhibited by Mg^{2+} (Movie S4). Without the addition of Mg^{2+}, cell growth of the ΔRLPAs Δ*cwlO* strain was normal (Movie S3). In WT cells or Δ*cwlO* cells, the presence of Mg^{2+} has no effect on cell viability or growth – growth is only inhibited in the absence of the RLPAs. Thus, the RLPAs appear to allow LytE to maintain its activity in the presence of Mg^{2+}.

To test whether LytE activity is directly inhibited by Mg^{2+}, we performed zymography with the addition of Mg^{2+} to the renaturation buffer on the Δ40 Δ*cwlO* strain, where LytE activity is easy to detect as it is the only remaining band (Figure 2A). Indeed, LytE activity was strongly reduced in the presence of 25 mM $MgCl_2$ (Figure 6B). Additionally, we reasoned that if the Mg^{2+}-sensitivity phenotype was due to direct inhibition of LytE by Mg^{2+}, increasing the levels of LytE should protect cells from death by increasing the total amount of LytE activity. Indeed, overexpression of LytE allowed cells to survive in the presence of higher levels of Mg^{2+}, although 100 mM $MgCl_2$ still inhibited growth (Figure 6C).

297 Thus, we conclude that LytE activity is inhibited by Mg^{2+} both *in vivo* and *in vitro*.
298 Furthermore, our data indicates that the RPLAs allow LytE to maintain normal function
299 in the presence of Mg^{2+}, though the specific mechanism is unclear. Whether the RLPAs
300 act directly or indirectly on LytE remains to be determined, but we anticipate that the
301 RLPAs interact with and activate LytE similar to what has been observed for the
302 *Mycobacterium smegatis* hydrolases RipA and RpfB: RipA's C-terminus (containing a
303 NLPC/P60 domain like LytE) interacts with RpfB's RlpA-like LTG domain (29), and RipA
304 and RpfB have synergistic activity *in vitro* (30). By analogy, LytE's catalytic NLPC/P60
305 domain may interact with the RlpA-like domains in YabE, YdjM, and YocH, leading to
306 increased LytE activity, allowing LytE to continue to function in the presence of Mg^{2+}.
307 The ΔRLPAs Δ*cwlO* strain also has increased sensitivity to ionic stress and low
308 temperatures, suggesting RLPAs might stimulate LytE activity under those conditions as
309 well.

310 **DISCUSSION**

311 Bacterial cell growth requires the action of PG hydrolases, but previous *in vivo*
312 hydrolase studies have been impeded by their diversity and redundancy. We
313 constructed and validated a *B. subtilis* strain lacking all hydrolases potentially involved
314 in cell growth besides LytE and CwlO. These deletions constitute 40 genes in total,
315 representing 10% of secreted proteins and 1% of all genes. The resulting Δ40 strain
316 enables the investigation of given hydrolases and the cellular contexts in which they
317 function, and in this work, allowed several new discoveries regarding their sufficiency,
318 regulation, and genetic interplay.

First, we found that not only is the Δ40 strain viable, it grows at the same rate as WT cells under standard lab growth conditions. This demonstrates that LytE and CwlO alone can function to expand the cell wall to allow cell growth. Furthermore, as single knockouts of LytE and CwlO in the Δ40 strain are viable and allow growth (albeit at a slightly reduced rates with some shape defects), this demonstrates *B. subtilis* requires only one of these two hydrolases to grow.

Second, the Δ40 strain allowed us to discover a yet-to-be-identified LTG which requires SweC for its activity in the Δ40 strain. Given that the only remaining candidate LTG we identified in the Δ40 strain is YrrL, it is likely that SweC is required for YrrL activity. As CwlO activity is dependent on SweC, and SweC forms a complex with SweD, FtsE, and FtsX (21), YrrL might be an additional member of this complex, and SweCD/FtsEX might regulate both YrrL and CwlO. These experiments demonstrate how the Δ40 strain can be used to interrogating the regulation or direct biochemical activity of any other *B. subtilis* hydrolase: as the majority of cell wall hydrolase activity is removed in the Δ40 strain, PG profiling can be used to identify the specific activities of individual hydrolases reintroduced back into the Δ40 background.

Likewise, our minimal hydrolase strain allowed us to show that RlpA-like lytic transglycosylases enhance LytE activity *in vivo* and that this enhancement can be important for growth under conditions where LytE activity is inhibited, including the presence of divalent cations, ionic stress, and cold. Although the mechanism for LytE enhancement is unclear, we hypothesize that RlpAs stimulate LytE activity via a direct interaction, as has been observed in *M. smegmatis* (30). Synthetic lethal or synthetic sick interactions are straightforward to identify and characterize in the Δ40 strain, giving

a useful tool to interrogate genetic relationships between different hydrolases or between hydrolases and other genes of interest – such as those involved in cell wall synthesis.

Surprisingly, the Δ40 strain grows normally under standard lab conditions. What, then, is the function of these 40 hydrolases, and why does *B. subtilis* encode so many of them? This multitude of hydrolases likely arises from the fact that hydrolases are involved in other processes aside from cell growth such as sporulation (4) and cell motility (31). Additionally, some hydrolases might be only be needed under nutrient conditions not tested here, such as during phosphate limitation where teichoic acids are not produced, where cells may require hydrolases that are not regulated by teichoic acids (32–34). Finally, these other hydrolases may be important during non-exponential growth states such as during stationary phase, where the recycling of cell wall turnover products, lacking in the Δ40 strain, reduces cell lysis (35). Thus, a broader screen of the sensitivity of the Δ40 strain in different nutrient and environmental conditions will allow researchers to determine which hydrolases are useful for which conditions.

In summary, the Δ40 minimal hydrolase strain provides a powerful experimental background to investigate the function, regulation, and interplay of hydrolases, improving our understanding of precisely how these enzymes conduct their cellular tasks. In the future, individual hydrolases can be reintroduced into the Δ40 strain to investigate their specific activities in the absence of confounding contributions from the other 39 genes. Using the Δ40 strain, PG profiling can determine the biochemical activity of hydrolases. Uncovering synthetic genetic interactions between hydrolases and other genes of interest – now easy to do for all 40 hydrolases at once – will allow us

365 to flesh out our understanding of bacterial cell growth. Understanding the function of cell
366 wall hydrolases is essential for a complete understanding of how bacteria grow, and the
367 Δ40 strain will allow rapid progress to this end.

368 **ACKNOWLEDGEMENTS**

369 We would like to thank Carl Wivagg, Alex Bisson, Matthew Holmes, Ferran
370 Garcia-Pichel, and Susanne Neuer for helpful advice and discussions, and Georgia
371 Squyres for both helpful advice, discussions, and reading of the manuscript. This work
372 was funded by National Institutes of Health Grants DP2AI117923-01 to ECG, as well as
373 support from the Volkswagen Foundation. This work was supported by the NSF-Simons
374 Center for Mathematical and Statistical Analysis of Biology at Harvard (1764269) and
375 the Harvard Quantitative Biology Initiative. Some work was performed at the Center for
376 Nanoscale Systems at Harvard University, supported by NSF ECS-0335765. HPLC-MS
377 work was performed by the Harvard Center for Mass Spectrometry Core Facility, and
378 sequencing was performed by the Bauer Core Facility at Harvard University.

379

METHODS

Strains, media, and growth conditions

Glycerol stocks stored at -80˚C were struck onto LB agar plates. For strain bSW61 (*lytE::pSpac-lytE, ΔcwlO*), these plates were additionally top spread with 1 mM IPTG. After incubation overnight at 37˚C, colonies were inoculated into 1 mL media and grown on a roller at 37˚C until they reached mid-exponential-phase growth (OD ~0.2). Cells were diluted 1:10 in prewarmed media and again grown until mid-exponential phase; this process was repeated until the start of the experiment. Alternately, a 1:10 dilution series of cells were grown overnight in media on a roller at 25˚C. The next day, the culture whose OD600 was nearest to 0.2 was diluted 1:10 and grown in media at 37˚C as above. $S7_{50}$AA indicates $S7_{50}$ media with added amino acids as in (36).

Strain construction

The wild type strain for this work was *B. subtilis* PY79. Strains used in this study are listed in Table S3. Constructs were created using Gibson assembly of PCR products. Linear Gibson assembly products were transformed into competent *B. subtilis*. Transformants were selected on LB plates containing the appropriate antibiotic. The resulting strains were verified by PCR. Constructs used in this study, as well as any plasmids used to create each construct, are listed in Table S3. Primers, along with strain construction details, are listed in Table S4. Resistance cassettes and promoters were amplified from purified plasmids (listed in Table S3), all other fragments were amplified from WT gDNA.

To combine knockouts, the parent strain was transformed with PCR product containing the locus (homology arms + resistance cassette) or gDNA as indicated. All

403 resistance cassettes used have loxP sites flanking the cassette, allowing Cre-based
404 loop out using plasmid pDR244 (a gift from David Rudner) of the cassette to yield a
405 markerless knockout. Removal of the plasmid was accomplished by shifting streaks to
406 42˚C where it cannot be replicated due to a temperature-sensitive origin. Successful
407 loop outs were confirmed via loss of antibiotic resistance.

408 **PHMMER search**

409 We used pfamscan version 1.6 to search the *B. subtilis* 168 and PY79 proteomes
410 for all pfam domains using default parameters: e-value: 0.01, significance E-values [hit]:
411 0.03, significance bit scores [sequence]: 25, significance bit scores [hit]: 22. We then
412 filtered the list for domains of interest, found in Table S3, and removed any cytoplasmic
413 proteins.

414 **PG purification, HPLC conditions, and MS data analysis**

415 PG purification was conducted as in (37), with the addition of a protein digestion
416 step. Cells were grown in a baffled flask to an OD of ~0.5 in 50 mL of CH media. Cells
417 were mixed 50/50 with 50 mL of boiling 10% SDS and boiled for 15 min in a water bath,
418 then pelleted at 5000x g and washed 5x with ddH2O. Cells were then resuspended in 2
419 mL DNAse/RNase buffer (10 mM Tris pH 7.5, 2.5 mM $MgCl_2$, 0.5 mM $CaCl_2$) with 20 uL
420 DNAse I and 20 uL RNAse A, then incubated overnight at 37˚C and washed 3x with
421 ddH2O to remove nucleic acids. Next, cells were resuspended in 2 mL Proteinase K
422 buffer (10 mM Tris pH 7.5, 1 mM $CaCl_2$) with 20 uL Proteinase K, incubated overnight at
423 45C, and washed 3x with ddH2O to remove proteins. Purified PG at this point was
424 ready for use in zymography as substrate. For PG profiling, the PG was resuspended in
425 12.5 mM $NaHPO_4$ pH 5.5 with 5000 units of mutanolysin and digested overnight (16h)

426 at 37˚C on a roller to yield soluble muropeptides. Undigested material was pelleted by
427 spinning at 16000x g for 5 mins and the supernatant was transferred to a new tube.
428 Soluble muropeptides were reduced with sodium borohydride (1 mg/mL) for 30 mins
429 and the reaction was stopped by adding 10 uL 30% phosphoric acid. The pH was
430 adjusted to 4-6 using NaOH, and the reduced soluble muropeptides were characterized
431 by high-resolution LC-MS operating in both positive and negative mode. Soluble
432 reduced muropeptides were separated on a Waters column with the following method:
433 column temperature 52˚C, flow rate 0.5 mL/min, linear gradient of solvent A (0.1%
434 formate) to 10% solvent B (acetonitrile + 0.1% formate) over 80 min.
435 Mass spectrometry data was analyzed using a custom MATLAB program,
436 available at https://bitbucket.org/garnerlab/wilson_40_2020/. For each compound, at
437 each time point, theoretical m/z values were compared with observed m/z with a cutoff
438 of 0.05 Da. Charge was determined from the isotopic distribution. To be considered a
439 match, each compound needed to have the appropriate charge, isotopic distribution,
440 and m/z value, and we required that a compound be present on both the positive and
441 negative scans. We filtered out any compounds that were less than 1% the abundance
442 of the most abundant species at each time point. Finally, if multiple compounds were
443 found at the same time point, the less abundant ones were filtered out.
444 **Zymography**
445 Zymography was performed as in (38), but using PG prepared as detailed under
446 PG purification. Purified PG was sonicated at max power on a sonicator for 2 min. A
447 15% polyacryamide bis-Tris gel was prepared with the purified PG. 50 mL of cells were
448 grown in a baffled flask with shaking to an OD of ~0.5. Cells were concentrated by

centrifugation at 5000x g for 5 min, resuspended in 1 mL of supernatant, then further concentrated by centrifugation at 16,000x g for 2.5 min. All media was aspirated, the centrifuge tube turned around, and centrifuged again at 16,000x g for 2.5 min. Cell wall binding proteins were extracted by resuspending the pellet in an equal volume of 8% SDS. This mixture was heated at 95˚C for 2 min then centrifuged at 16,000x g for 2.5 min. The supernatant was transferred to a new tube, 6x SDS-PAGE Laemmli buffer was added, and the extracted proteins were loaded on the gel. Gels were run in SDS-MOPS buffer at constant amps (20 mA) for 4-6 hours, then washed with ddH2O, and placed in renaturation solution (1% Triton-X 100, 25 mM Tris pH 7.5). The gel was incubated for 16h at 37C with gentle shaking, then stained 4h with a methylene blue staining solution (1% methylene blue, 0.1% KOH), washed several times with ddH2O, and destained overnight in 500 mL ddH2O with gentle shaking. Gels were photographed using a Canon SC1011 scanner in a standard plastic page protector.

Growth rates

Cells were grown to an OD of ~0.3-0.5 on a roller drum at 37˚C and diluted to an OD of ~0.05 in baffled flasks in a water bath shaker at 37˚C. Samples were withdrawn at 5 min intervals and OD was measured in a plastic cuvette using a Biowave Cell Density Meter CO8000. T vs. OD curves were fit to a single exponential ($OD = Ae^{BT}$) to extract a growth rate (B).

Turnover rates

Cells were grown in $S7_{50}AA$ to an OD of ~0.3-0.5 on a roller drum at 37˚C and diluted to an OD of ~0.05 in 3 mL of prewarmed media containing 1 uCi of ^{3}H-N-acytylglucosamine (specific activity: 20 Ci/mmol, American Radiolabeled Chemicals,

Inc., St. Louis, MI, USA) in 25mm wide test tubes in a water bath shaker at 37˚C. Cells were labeled for 3 generations (OD ~0.4), then filtered, washed twice with prewarmed media, and resuspended in 25 mL of prewarmed media. Samples were withdrawn at 5 min intervals and OD was measured in a plastic cuvette using a Biowave Cell Density Meter CO8000. Samples were mixed 50:50 with ice cold 10% TCA + 20 mM unlabeled GlcNAc, incubated on ice for 10 mins, then filtered and washed. Filters were dried, resuspended in Ultima Gold LSC cocktail (PerkinElmer, Waltham, MA, USA) and radioactivity was measured using a scintillation counter (Tri-Carb 2100 TR, PerkinElmer). Counts/min vs. OD plots were fit to a single exponential ($CPM = Ae^{BT}$) to extract a turnover rate (B).

Cell dimensions

Cells were grown to an OD of ~0.3-0.5 in a water bath shaker at 37˚C. 1 mL of culture was stained with FM 5-95 and concentrated to 100 uL by centrifugation at 2000x g and resuspension. 5 uL of concentrated cells were spotted under 2% agarose pads in CH containing 0.5 ug/mL FM 5-95. Images were collected on a Nikon Ti-E microscope using a Nikon CFI Plan Apo DM Lambda 100X Oil objective, 1.45 NA, phase ring Ph3 using an ORCA-Flash4.0 V2 sCMOS camera. Analysis was performed using Morphometrics v1.1 (39). Zero length or width cells were discarded, as well as any cells with width greater than length. Outliers were removed using Graphpad Prism ROUT with default parameters (1%).

Electron microscopy and cell wall thickness

Electron microscopy was performed as in (40). Briefly, exponentially growing cells were fixed in 100 mM MOPS buffer pH 7 containing 2% paraformaldayde, 2.5%

gluteraldehyde, and 1% dimethyl sulfoxide overnight at 4°C, washed, stained with 2% osmium tetroxide in 100 mM MOPS for 1 hr, washed, and stained overnight with 2% uranyl acetate. The cells were then dehydrated and embedded in Embed 812 resin.

Serial ultrathin sections (80 nm) were cut with a Diatome diamond knife (EMS, PA) on a Leica Ultracut UCT (Leica Microsystems, Germany) and collected on 200-mesh thin-bar formvar carbon grids. Sections were imaged on a Hitatchi HT7800 transmission electron microscope.

Images collected were segmented (inner cell wall, outer cell wall) using DeepCell (41), and cell wall thickness was measured using a custom Matlab program available at https://bitbucket.org/garnerlab/wilson_40_2020/. Briefly, the distance between the inner and outer cell wall was measured every 10 nm along a user-defined line, and the mean of that measurement was taken to be the cell's cell wall thickness.

Spot dilution assay

Cells were grown to an OD of 0.5 and diluted 1:10 into 100 uL of LB media in a 96 well plate. A 1:10 serial dilution series was made, and 3 uL of each dilution was spotted onto the plate using a multichannel pipettor. The plates were allowed to dry and incubated in at 37˚C or 42˚C as indicated for 18h. Plates incubated at 25˚C or 18˚C were left for additional time (24h and 48h, respectively). Plates were photographed using a Canon SC1011 scanner with the lid open.

For the colony morphology assay in Figure 1, this protocol was followed except that a colony of cells of each strain were simply resuspended in 100 uL of media using a toothpick (omitting the broth culture step).

Data availability

518 All custom software used in this work is available at

519 https://bitbucket.org/garnerlab/wilson_40_2020/. Raw HPLC-MS data for PG profiling

520 experiments available from ftp://massive.ucsd.edu/MSV000086886

521 (doi:10.25345/C5R21D). Raw and error corrected sequencing reads for whole genome

522 sequencing available at https://www.ncbi.nlm.nih.gov/Traces/study/?acc=PRJNA702153

523 (BioProject PRJNA702153).

524

525

Name (alias)	PY79	UniProt	Locus tag	Regulons	e-value	References	Activity
AMIDASE							
Amidase_2 (PF01510)							
cwlA	Y/KO	P24808	BSU25900		5.60E-19	(42–44)	
cwlH (yqeE)	Y/KO	P54450	BSU25710	gerE^*, sigK^*	7.50E-25	(45)	
xlyA	Y/KO	P39800	BSU12810	xpf*	1.00E-23	(46)	
xlyB (yjpB)	Y/KO	O34391	BSU12460		2.20E-18	similarity; xlyA	
blyA (yomC)	N	O31982	BSU21410		2.30E-18	(47)	
Amidase_3 (PF01520)							
cwlC	Y/KO	Q06320	BSU17410	sigK^*	3.4E-44	(48, 49)	
cwlD	Y/KO	P50864	BSU01530	lexA^*, sigE^*, sigG^*	1.10E-48	(19, 50, 51)	
lytC (cwlB)	Y/KO	Q02114	BSU35620	sigA^*, sigD^*, sinR^*, slrR^*, yvrHB^*	6.4E-54	(7, 49, 52–54)	
yqiI	Y/KO	P54525	BSU24190	sigA*	5.50E-56	(55)	
yrvJ	Y/KO	O32041	BSU27580	sigH^	2.30E-44	similarity; lytC	
Amidase_6 (PF12671)							
yhbB (ygaQ)	Y/KO	O31589	BSU08920	sigE^*	1.50E-39	uncharacterized	
yjcM	Y/KO	O31635	BSU11910	abrB*, sigD*	1.30E-23	uncharacterized	
SpoIIP (PF07454)							
spoIIP	Y/KO	P37968	BSU25530	sigE^*, sigF^*, sigG^*, spoVT^*	9.70E-79	(56, 57)	amidase, DDEP
Beta-lactamase (PF00144)							
pbpE	Y/KO	P32959	BSU34440	sigW^*	3.40E-61	(58)	not shown
pbpX	Y/KO	O31773	BSU16950	sigM^*, sigV^*, sigW^, sigX^*	7.90E-54	similarity; pbpE	
amiE (ybbE)	Y	O05213	BSU01670	murR*	7.40E-76	does not hydrolyse PG (14)	
N-ACETYLGLUCOSAMIDASE/LYTIC TRANSGLYCOSYLASE							
Glyco_hydro_3 (PF01915)							
nagZ (yzbA, ybbD)	Y	P40406	BSU01660	murR*	6.50E-131	does not hydrolyse PG (14)	
Glyco_hydro_18 (PF00704)							
yaaH (sleL)	Y/KO	P37531	BSU00160	sigB^*, sigE^*, spoIIID^*	1.20E-26	cleaves small fragments (59–61)	
ydhD	Y/KO	O05495	BSU05710	sigE^*	9.60E-30	similarity; yaaH	
ykvQ	Y/KO	O31682	BSU13790	sigK^*	2.50E-23	similarity; yaaH	
yvbX	Y/KO	O32258	BSU34020		1.10E-33	similarity; yaaH	

				Glucosaminidase (PF01832)			
lytD (cwlG)	Y/KO	P39848	BSU35780	sigD^*, sigG^	3.30E-11	(7, 62, 63)	
lytG	Y/KO	O32083	BSU31120		6.80E-24	(64)	
				3D (PF06725)			
yabE	Y/KO	P37546	BSU00400	sigA*	1.80E-22	similarity; yuiC, yocH	probably LTG
yocH	Y/KO	O34669	BSU19210	abrB^*, sigA^*, spo0A^*, walR^*	3.50E-22	(28)	probably LTG
yuiC	Y/KO	O32108	BSU32070	codY^*, sigF^*	9.40E-21	(65)	probably LTG
yorM	N	O31901	BSU20330		7.90E-11	similarity; yuiC, yocH	probably LTG
				Hydrolase_2 (PF07486)			
cwlJ (ycbQ)	Y/KO	P42249	BSU02600	sigE^*, sigK^*, spoIIID^*	1.60E-18	(66)	probably LTG
sleB (ypeA)	Y/KO	P50739	BSU22930	sigG^*	1.20E-25	(67–69)	probably LTG
ykvT	Y/KO	O31685	BSU13820	walR*	5.80E-28	similarity; sleB, cwlJ	probably LTG
				SLT (PF01464)			
xkdO	Y/KO	P54334	BSU12680	xpf*	6.20E-20	similarity; cwlQ, cwlP	probably LTG
cwlQ (yjbJ)	Y/KO	O31608	BSU11570	sigD^*	1.70E-34	(70, 71)	LTG + muramidase
yqbO	Y/KO	P45931	BSU26030		5.70E-24	similarity; cwlQ, cwlP	probably LTG
cwlP (yomI)	Y/KO	O31976	BSU21350		1.80E-32	(72)	muramidase, DDEP
				Lysozyme_like (PF13702)			
yocA	Y/KO	O34636	BSU19130		4.30E-59	similarity; CwlT	probably muramidase
cwlT (yddH)	N	P96645	BSU04970	immR*	2.10E-42	(73)	muramidase, DLEP
				DPBB_1 (PF03330)			
ydjM (yzvA)	Y/KO	P40775	BSU06250	phoP*, walR*	1.00E-09	similarity; PaRlpA (74)	probably LTG
yoaJ (EXLX1)	N	O34918	BSU18630	fur*	2.90E-07	does not hydrolyse PG (75)	
				SpoIID (PF08486)			
spoIID (spoIIC)	Y/KO	P07372	BSU36750	sigE^*, spoIIID^*	1.30E-23	(56, 76)	LTG
lytB (cwbA)	Y	Q02113	BSU35630	sigA^*, sigD^*, sinR^*, slrR^*, yvrHB^*	3.90E-23	does not hydrolyse PG (77, 78)	
				YceG (PF02618)			
yrrL (mltG)	Y	O34758	BSU27370	spo0A^*	3.20E-90	similarity; EcMltG (20)	probably LTG
sweC (yqzC)	Y	O32023	BSU24940	spo0A^*	1.40E-07	similarity; EcMltG (20)	

PEPTIDASE							
DL-endopeptidase							
				NLPC/P60 (PF00877)			
cwlO (yzkA,yvcE)	Y	P40767	BSU34800	sigA*, walR*	4.40E-29	(16)	DLEP
cwlS (yojL)	Y/KO	O31852	BSU19410	abh^*, abrB^*, ccpA^*, sigD^*, sigH^*	4.70E-29	(11)	DLEP
lytE (papQ, cwlF)	Y	P54421	BSU09420	sigA^*, sigH^*, sigI^*, spo0A^*, walR^*	3.30E-28	(79, 80)	DLEP
lytF (cwlE, ydhD)	Y/KO	O07532	BSU09370	sigD^*, sinR^*, slrR^*	1.40E-28	(81, 82)	DLEP
pgdS (ywtD)	Y	P96740	BSU35860	sigD^*	1.00E-22	does not hydrolyze PG (83)	
ykfC	Y/KO	O35010	BSU12990	codY*	1.80E-29	(84)	DLEP
cwlT (yddH)		P96645	BSU04970	immR*	3.50E-34	(73)	
				Peptidase_M14 (PF00246)			
yqgT	Y/KO	P54497	BSU24830		2.70E-27	similarity to B. sphaericus EP1, (85)	probably DLEP
				Peptidase_C92 (PF05708)			
yycO	Y/KO	Q45607	BSU40280	sigK^*	5.0E-5		
LD-endopeptidase							
				Peptidase_M15 (PF01427)			
cwlK (ycdD)	Y/KO	O34360	BSU02810		3.10E-20	(86)	LDEP
				Peptidase_M23 (PF01551)			
lytH (yunA, yutA)	Y/KO	O32130	BSU32340	sigK^*	1.80E-21	(87)	LDEP
spoIIQ	Y	P71044	BSU36550	sigF^*	1.00E-24	no evidence for PG hydrolysis	
spoIVFA	Y	P26936	BSU27980	sigE^*, spoIIID^*	3.40E-12	no evidence for PG hydrolysis	
cwlP (yomI)	N	O31976	BSU21350		1.80E-27	(72)	muramidase, DD-EP

526 **Table 1: List of cell wall hydrolases in *Bacillus subtilis* identified using PHMMER.**

Cell wall hydrolases were identified via a PHMMR (13) search with default parameters of the *B. subtilis* subsp. 168 and *B. subtilis* subsp. PY79 proteome for PFAM domains associated with known cell wall hydrolases (Table S2). For each hydrolase, we report its name (and any aliases), whether it is knocked out in the Δ40 strain (KO) or present in PY79 (Y/N), its UniProt accession number, its locus tag, any reported regulons it is a member of (^ indicates source Faria et al. 2016, * indicates source SubtiWiki), the PHMMR search significance e-value, and any relevant references showing its biochemical activity. Abbreviations: DLEP, D,L-endopeptidase; LDEP, L,D-endopeptidase; LTG, lytic transglycosylase.

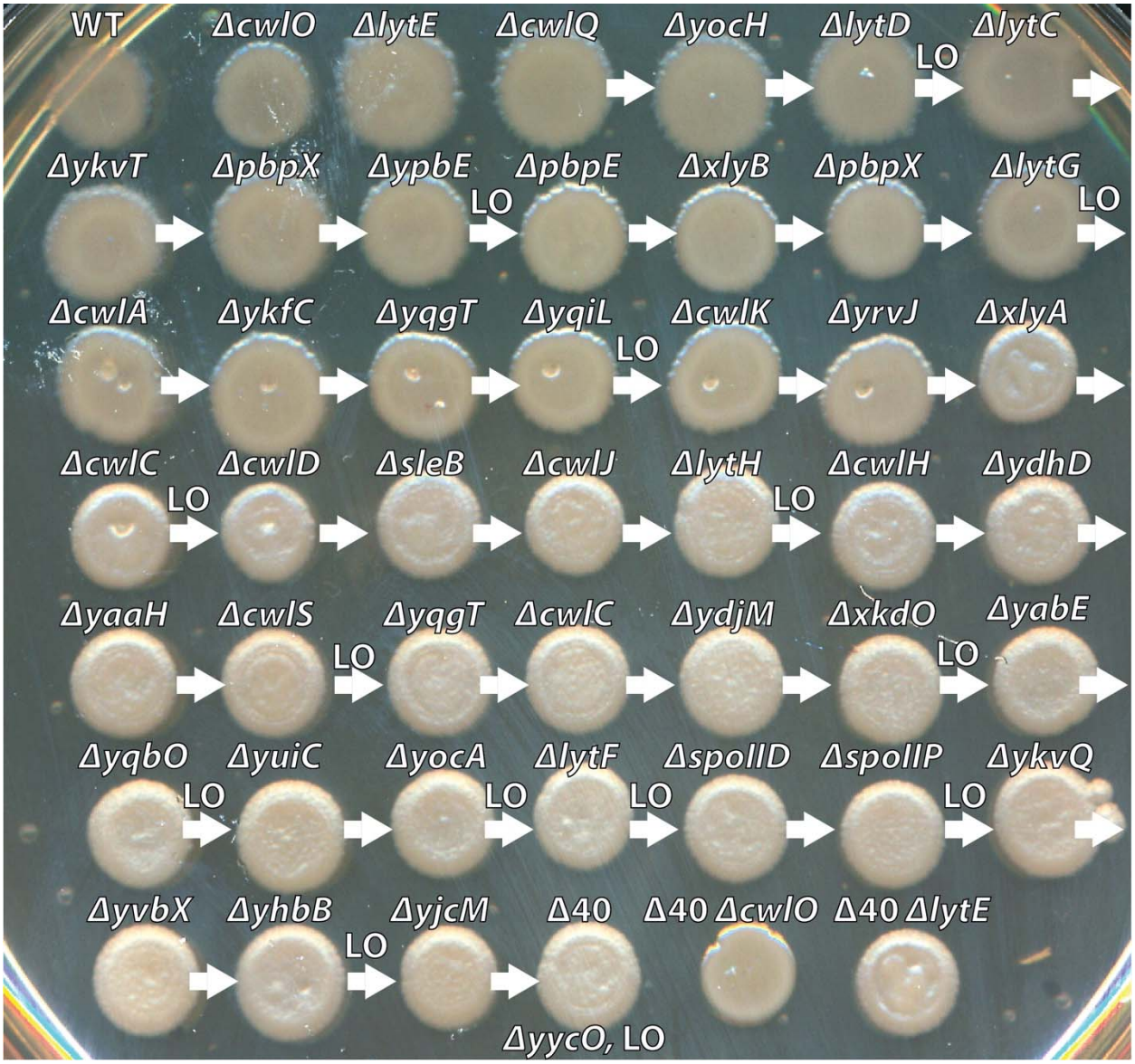

Figure 1: Construction of the Δ40 strain via sequential knockout and loopout. Colony morphology of each cloning intermediate for the Δ40 strain. WT cells were transformed with a series of resistance-cassette-marked knockouts (starting with Δ*cwlQ*). Periodically, antibiotic resistance cassettes were removed via Cre-loxP mediated loopout (indicated by LO). Arrows indicate sequential integrations (e.g., the strain indicated by Δ*yocH* contains Δ*yocH* and Δ*cwlQ*). Dense cell suspensions were spotted and incubated overnight to visualize colony morphology.

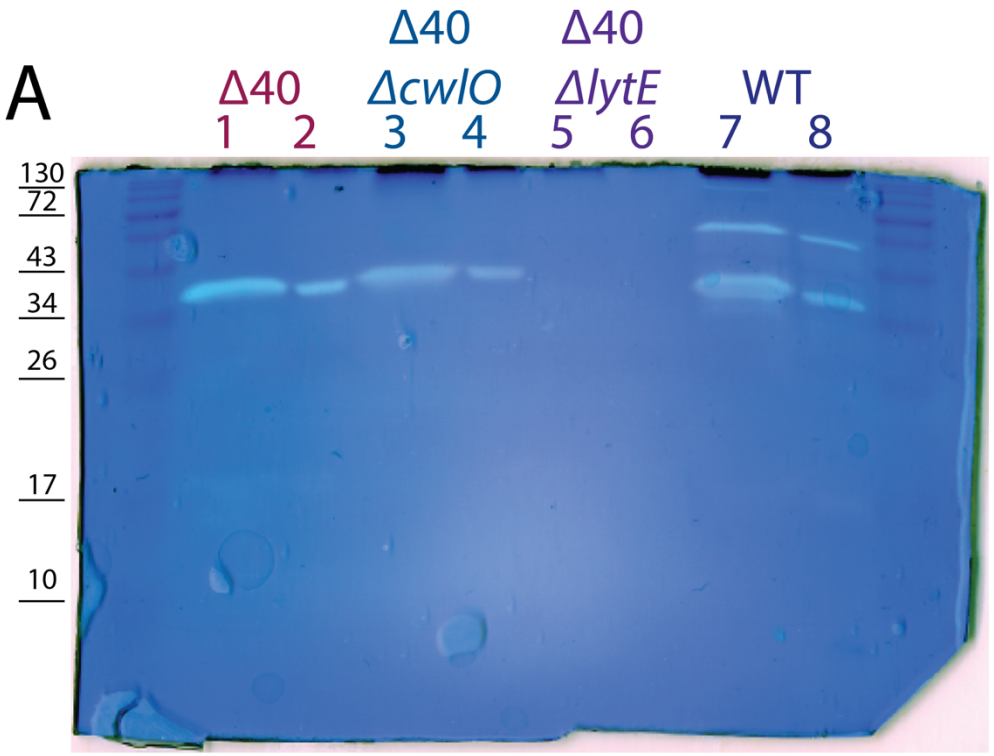

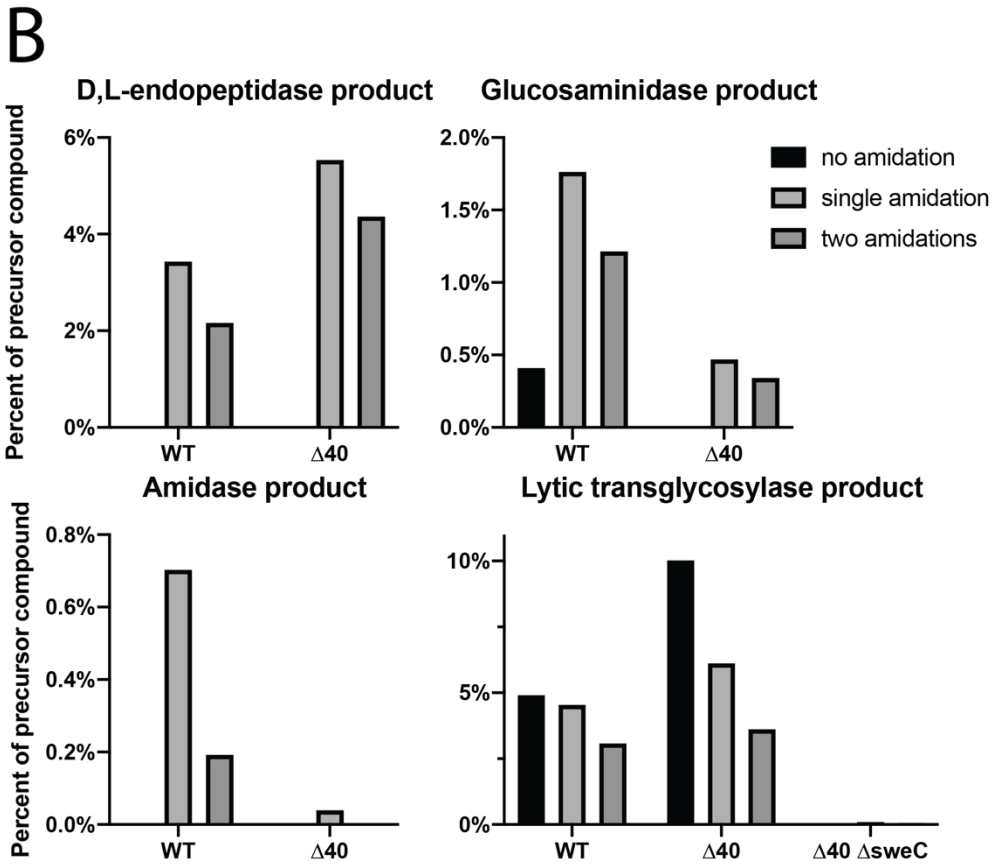

Figure 2: The Δ40 strain has a substantially reduced cell wall hydrolytic complement

A: Only LytE activity is visible by zymography in the Δ40 strain. Zymography (renaturing SDS-PAGE gel using purified *B. subtilis* cell walls as substrate) was performed as described in Methods. The activity of cell wall hydrolases causes clearing of the gel. In each pair of lanes, the first was loaded with 20 µL of cell wall binding protein extract, and the second with 5 µL. Several major and minor bands of cell wall hydrolytic activity are visible in the wild type strain (strain PY79, lanes 7 and 8). Only one band of cell wall hydrolytic activity is visible in the Δ40 mutant (strain bSW431, lanes 1 and 2). This band is still visible when *cwlO* is knocked out in the Δ40 strain (Δ40 Δ*cwlO*, strain bSW433, lanes 3 and 4) but disappears in the reciprocal *lytE* knockout (Δ40 Δ*lytE*, strain bSW435, lanes 5 and 6). Thus, this band represents LytE activity.

B: Identification of cell wall hydrolase products in WT and Δ40 cells by peptidoglycan profiling. Purified cell walls were digested to yield soluble muropeptides which were separated and characterized via HPLC-MS (see Methods for details). The abundance of each cell wall hydrolase product was normalized by the abundance of its precursor compound; each product contains two mDAP residues, and each mDAP can be amidated, so these species were compared separately (for example, the abundance of singly amidated glucosaminidase product was divided by the abundance of singly amidated crosslinked PG, its immediate biochemical precursor). D,L-endopeptidase products are still present as expected, because the strain retains the D,L-endopeptidases LytE and CwlO. Amidase products are largely absent. Glucosaminidase products are substantially reduced in abundance. Lytic

569 transglycosylase products are still present in the Δ40 strain but disappear if *sweC* is
570 additionally knocked out. Thus, the Δ40 strain is deficient for several major classes of
571 cell wall hydrolase activity. Strains used: PY79, WT; bSW431, Δ40; bSW537, Δ40
572 Δ*sweC*.

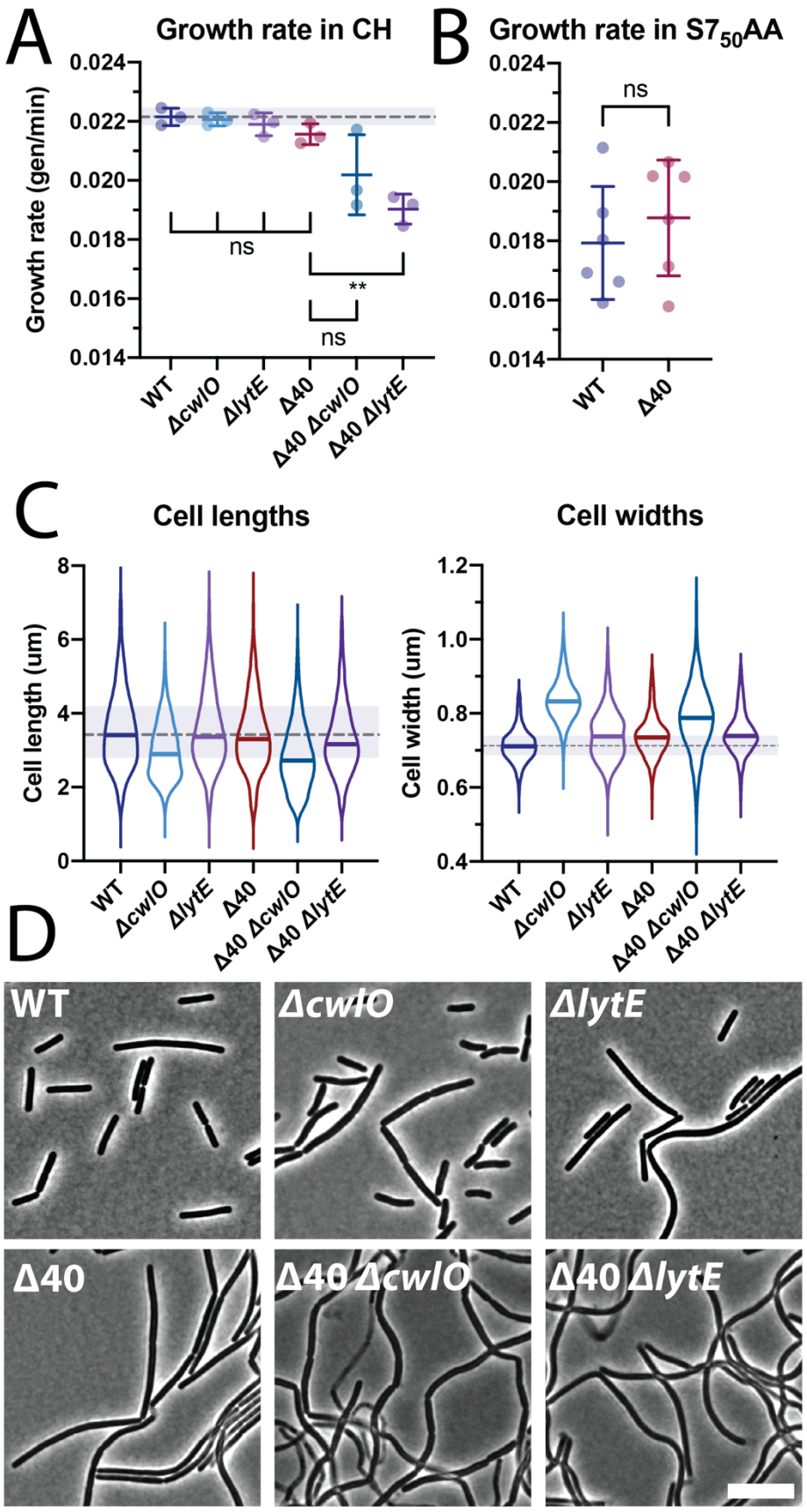

574 **Figure 3: The Δ40 strain grows at a similar rate as WT cells and has mild shape**
575 **defects.**

576 **A: The Δ40 strain has a similar growth rate to WT in rich media.** Cultures were
577 grown in CH media at 37˚C to an OD of ~0.3-0.5, diluted to an OD of 0.05, and samples
578 were collected every 6 minutes for 1.5 hrs (~3 doublings). OD_{600} vs time plots were fit to
579 a single exponential to obtain the growth rate. Each point represents the doubling time
580 from a single experiment, and solid lines show mean and standard deviation. The dotted
581 line shows the mean WT growth rate, for comparison. While Δ40 has a similar growth
582 rate to WT, *lytE* and *cwlO* knockouts grow more slowly in this background than in a WT
583 background. Strains used: PY79, WT; bSW23, Δ*cwlO*; bSW295, Δ*lytE*; bSW431, Δ40;
584 bSW433, Δ40 Δ*cwlO*; bSW435, Δ40 Δ*lytE*.

585 **B: The Δ40 strain has a similar growth rate to WT in minimal media.** Cultures were
586 grown in $S7_{50}$AA media at 37˚C. Samples were collected and data was analyzed as in
587 (A). Strains used: PY79, WT; bSW431, Δ40.

588 **C: Cell lengths (left) and widths (right) in hydrolase mutants.** Cells were labeled
589 with membrane stain and imaged by epifluorescence microscopy. Cell dimensions were
590 measured from these images using Morphometrics. Solid lines in violins show medians.
591 Dashed line outside violins shows WT median for comparison. Shaded region outside
592 violins shows WT quartiles. Strains used: PY79, WT; bSW23, Δ*cwlO*; bSW295, Δ*lytE*;
593 bSW431, Δ40; bSW433, Δ40 Δ*cwlO*; bSW435, Δ40 Δ*lytE*.

594 **D: Representative phase contrast images of hydrolase mutant strains.** Δ40 cells
595 primarily form long chains, Δ40 Δ*cwlO* cells have variable widths, and Δ40 Δ*lytE* cells
596 sometimes have phase-light, lysed cells still attached to their poles (see Figure S2 for

597 TEM images). Both Δ40 Δ*cwlO* and Δ40 Δ*lytE* have a population of phase-light, lysed
598 cells. Scale bar is 10 μm.

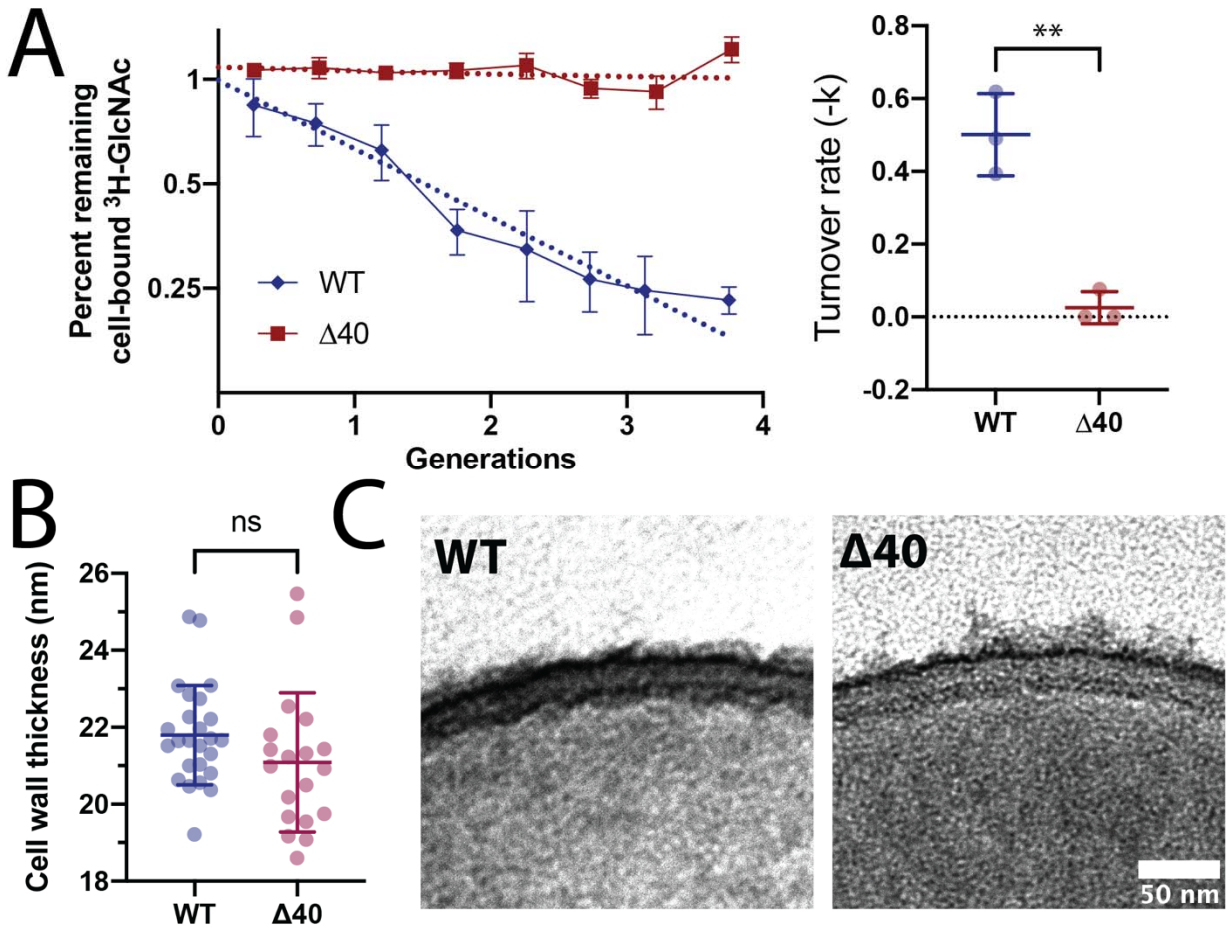

599

600 **Figure 4: The Δ40 strain has no increase in cell wall thickness and does not turn**
601 **over cell wall.**

602 **A: Cell wall turnover rate is negligible in the Δ40 strain.** *Left*: Pulse-chase radiolabel
603 measurements were used to determine the cell wall turnover rate. Cells were labeled
604 with H^3-GlcNAc, which incorporates into the cell wall. The ^{3}H-GlcNAc was then washed
605 out and radioactivity was subsequently measured for 3 generations. A decrease in
606 radioactivity indicates that material is being removed from the cell wall, e.g. that cell wall
607 is turning over. Each experiment was replicated at least 3 times. Dotted lines show

608 single exponential fit to mean data. *Right*: Single exponential fits to each experiment at
609 left. Each point represents the time constant (-k) obtained from a fit to a single
610 experiment. Error bars show SD. The Δ40 turnover rate is not significantly different from
611 zero (one sample t test, p=0.4837). Strains used: PY79, WT; bSW431, Δ40.
612 **B: Cell wall thickness in the Δ40 strain is similar to WT.** Cell wall thickness was
613 measured via transmission electron microscopy as described in Methods. Briefly,
614 exponentially growing cells were fixed, osmicated, stained with uranyl acetate,
615 embedded in Embed 812, sectioned, and imaged without additional staining. Each point
616 is the mean cell wall thickness measured for a single cell. Error bars show SD. Strains
617 used: PY79, WT; bSW431, Δ40.
618 **C: Representative images of cell wall thickness.** Representative images of cell wall
619 thickness analyzed in C. Strains used: PY79, WT; bSW431, Δ40. Scale bar is 50 nm.
620

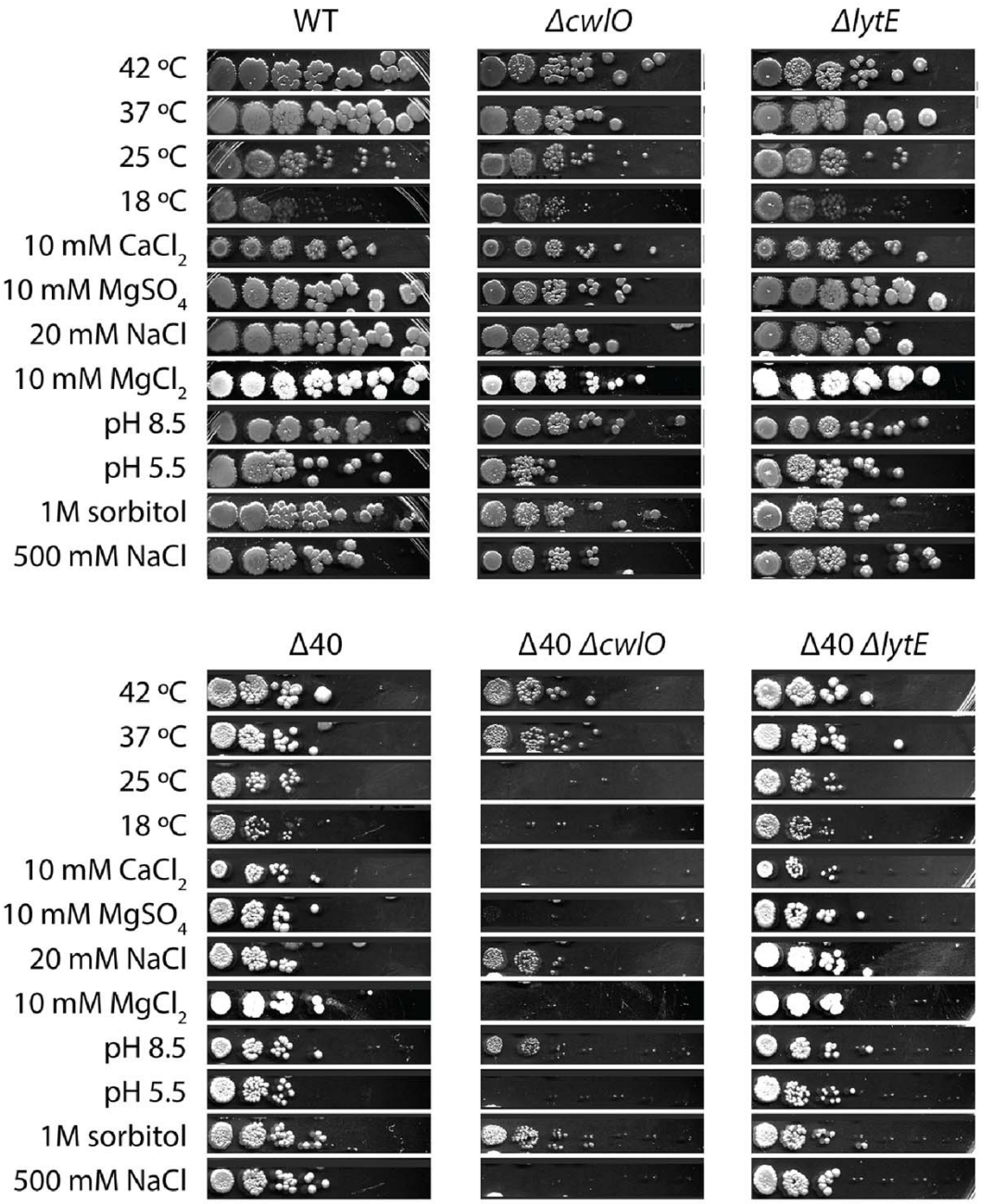

Figure 5: The Δ40 strain has similar viability to WT in a range of stress conditions, but Δ40 Δ*cwlO* is sensitive to ionic, cold, and low pH stress. Spot dilution assays of different strains under various stress conditions. Cultures of each strain were plated in a 1:10 dilution series onto LB plates containing various stressors and grown overnight at the specified temperature, or at 37˚C if not indicated. Most conditions supported normal

627 growth, but growth of the Δ40 Δ*cwlO* strain was inhibited at 25˚C, pH 5.5, or with the
628 addition of 10 mM $MgCl_2$, 10 mM $MgSO_4$, 10 mM $CaCl_2$, or 300 mM NaCl. Strains used:
629 PY79, WT; bSW23, Δ*cwlO*; bSW295, Δ*lytE*; bSW431, Δ40; bSW433, Δ40 Δ*cwlO*;
630 bSW435, Δ40 Δ*lytE*.
631
632
633

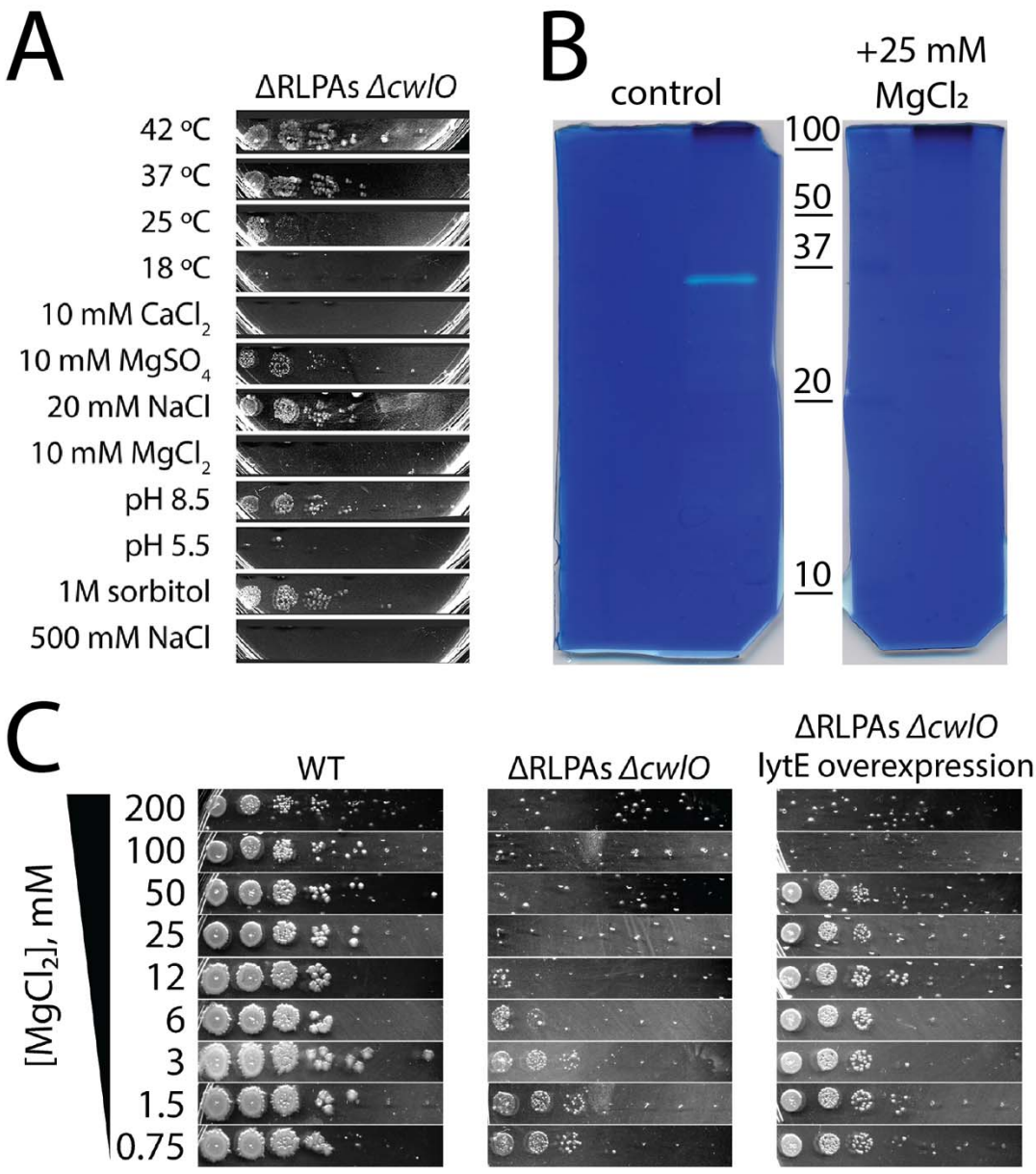

Figure 6: Three uncharacterized RlpA-like proteins stimulate LytE activity in the presence of divalent cations.

A: The removal of three RlpA-like proteins makes Δ*cwlO* cells stress-sensitive. Spot dilution assays were performed as in Figure 4. Δ*yabE* Δ*yocH* Δ*ydjM* (ΔRLPAs) Δ*cwlO* showed the same stress sensitivity profile as Δ40 Δ*cwlO*, except that 10 mM

640 $MgSO_4$ and 25˚C only partially inhibited growth. Strain used: bSW490, Δ*cwlO* Δ*yabE*
641 Δ*yocH* Δ*ydjM*.
642 **B: Mg^{2+} directly inhibits LytE activity.** Zymography was performed on Δ40 Δ*cwlO*
643 cells as in Figure 1A, but with the addition of the indicated concentration of $MgCl_2$ to the
644 renaturation buffer. 25 mM $MgCl_2$ almost completely inhibited the activity of LytE. Strain
645 used: bSW433, Δ40 Δ*cwlO.*
646 **C: LytE overexpression rescues Mg^{2+} sensitivity in the ΔRLPAs Δ*cwlO***
647 **background.** Spot dilutions were performed as in Figure 5A, with the indicated
648 concentration of $MgCl_2$ and the addition of 1 mM IPTG to drive LytE overexpression.
649 Strains used: PY79, WT; (ΔRLPAs) Δ*cwlO*, bSW490, Δ*cwlO* Δ*yabE* Δ*yocH* Δ*ydjM*;
650 (ΔRLPAs) Δ*cwlO* lytE overexpression, bSW519, Δ*cwlO* Δ*yabE* Δ*yocH* Δ*ydjM*
651 *amyE::pHyperSpank-lytE*.
652
653

REFERENCES

1. Brill J, Hoffmann T, Bleisteiner M, Bremer E. 2011. Osmotically controlled synthesis of the compatible solute proline is critical for cellular defense of Bacillus subtilis against high osmolarity. J Bacteriol 193:5335–5346.
2. Vollmer W. 2012. Bacterial growth does require peptidoglycan hydrolases. Mol Microbiol 86:1031–1035.
3. Typas A, Banzhaf M, Gross CA, Vollmer W. 2012. From the regulation of peptidoglycan synthesis to bacterial growth and morphology. Nat Rev Microbiol 10:123–136.
4. Smith TJ, Blackman SA, Foster SJ. 2000. Autolysins of Bacillus subtilis: Multiple enzymes with multiple functions. Microbiology 146:249–262.
5. Vermassen A, Leroy S, Talon R, Provot C, Popowska M, Desvaux M. 2019. Cell wall hydrolases in bacteria: Insight on the diversity of cell wall amidases, glycosidases and peptidases toward peptidoglycan. Front Microbiol 10.
6. Dik DA, Marous DR, Fisher JF, Mobashery S. 2017. Lytic transglycosylases: concinnity in concision of the bacterial cell wall. Crit Rev Biochem Mol Biol 52:503–542.
7. Blackman SA, Smith TJ, Foster SJ. 1998. The role of autolysins during vegetative growth of Bacillus subtilis 168 73–82.
8. Holtje J V. 1995. From growth to autolysis: The murein hydrolases in Escherichia coli. Arch Microbiol 164:243–254.
9. Heidrich C, Ursinus A, Berger J, Schwarz H, Höltje JV. 2002. Effects of multiple deletions of murein hydrolases on viability, septum cleavage, and sensitivity to

677 large toxic molecules in Escherichia coli. J Bacteriol 184:6093–6099.
678 10. Bisicchia P, Noone D, Lioliou E, Howell A, Quigley S, Jensen T, Jarmer H, Devine
679 KM. 2007. The essential YycFG two-component system controls cell wall
680 metabolism in Bacillus subtilis. Mol Microbiol 65:180–200.
681 11. Fukushima T, Afkham A, Kurosawa SI, Tanabe T, Yamamoto H, Sekiguchi J.
682 2006. A new D,L-endopeptidase gene product, YojL (renamed CwlS), plays a role
683 in cell separation with LytE and LytF in Bacillus subtilis. J Bacteriol 188:5541–
684 5550.
685 12. Meisner J, Montero Llopis P, Sham LT, Garner E, Bernhardt TG, Rudner DZ.
686 2013. FtsEX is required for CwlO peptidoglycan hydrolase activity during cell wall
687 elongation in Bacillus subtilis. Mol Microbiol 89:1069–1083.
688 13. Potter SC, Luciani A, Eddy SR, Park Y, Lopez R, Finn RD. 2018. HMMER web
689 server: 2018 update. Nucleic Acids Res 46:W200–W204.
690 14. Litzinger S, Duckworth A, Nitzsche K, Risinger C, Wittmann V, Mayer C. 2010.
691 Muropeptide rescue in Bacillus subtilis involves sequential hydrolysis by β-N-
692 acetylglucosaminidase and N-acetylmuramyl-L-alanine amidase. J Bacteriol
693 192:3132–3143.
694 15. Foster SJ. 1992. Analysis of the Autolysins of Bacillus subtilis 168 during
695 Vegetative Growth and Differentiation by Using Renaturing Polyacrylamide Gel
696 Electrophoresis 174:464–470.
697 16. Yamaguchi H, Furuhata K, Fukushima T, Yamamoto H, Sekiguchi J. 2004.
698 Characterization of a new Bacillus subtilis peptidoglycan hydrolase gene, yvcE
699 (named cwlO), and the enzymatic properties of its encoded protein. J Biosci

Bioeng 98:174–181.

17. Hashimoto M, Ooiwa S, Sekiguchi J. 2012. Synthetic lethality of the lytE cwlO genotype in Bacillus subtilis is caused by lack of D,L-endopeptidase activity at the lateral cell wall. J Bacteriol 194:796–803.

18. Williamson MP, Atrih A, Bacher G, Foster SJ. 1999. Analysis of Peptidoglycan Structure from Vegetative Cells of. Society 181:3956–3966.

19. Atrih A, Zöllner P, Allmaierr G, Foster SJ. 1996. Structural analysis of Bacillus subtilis 168 endospore peptidoglycan and its role during differentiation. J Bacteriol 178:6173–6183.

20. Yunck R, Cho H, Bernhardt TG. 2016. Identification of MltG as a potential terminase for peptidoglycan polymerization in bacteria. Mol Microbiol 99:700–718.

21. Brunet YR, Wang X, Rudner DZ. 2019. SweC and SweD are essential co-factors of the FtsEX-CwlO cell wall hydrolase complex in Bacillus subtilis. PLoS Genet 15:1–27.

22. Pooley HM. 1976. Layered distribution, according to age, within the cell wall of Bacillus subtilis. J Bacteriol 125:1139–1147.

23. Fan DP, Beckman MM. 1971. Mutant of Bacillus subtilis demonstrating the requirement of lysis for growth. J Bacteriol 105:629–636.

24. Kern T, Giffard M, Hediger S, Amoroso A, Giustini C, Bui NK, Joris B, Bougault C, Vollmer W, Simorre JP. 2010. Dynamics characterization of fully hydrated bacterial cell walls by solid-state NMR: Evidence for cooperative binding of metal ions. J Am Chem Soc 132:10911–10919.

25. Matias VRF, Beveridge TJ. 2005. Cryo-electron microscopy reveals native

723 polymeric cell wall structure in Bacillus subtilis 168 and the existence of a
724 periplasmic space. Mol Microbiol 56:240–251.
725 26. Hussain S, Wivagg CN, Szwedziak P, Wong F, Schaefer K, Izoré T, Renner LD,
726 Holmes MJ, Sun Y, Bisson-Filho AW, Walker S, Amir A, Löwe J, Garner EC.
727 2018. MreB filaments align along greatest principal membrane curvature to orient
728 cell wall synthesis. Elife 7:1–45.
729 27. Formstone A, Errington J. 2005. A magnesium-dependent mreB null mutant:
730 Implications for the role of mreB in Bacillus subtilis. Mol Microbiol 55:1646–1657.
731 28. Shah IM, Dworkin J. 2010. Induction and regulation of a secreted peptidoglycan
732 hydrolase by a membrane Ser/Thr kinase that detects muropeptides. Mol
733 Microbiol 75:1232–1243.
734 29. Hett EC, Chao MC, Rubin EJ. 2010. Interaction and modulation of two
735 antagonistic cell wall enzymes of mycobacteria. PLoS Pathog 6:1–14.
736 30. Hett EC, Chao MC, Deng LL, Rubin EJ. 2008. A mycobacterial enzyme essential
737 for cell division synergizes with resuscitation-promoting factor. PLoS Pathog 4.
738 31. Sanchez S, Dunn CM, Kearns DB. 2021. CwlQ is required for swarming motility
739 but not flagellar assembly in Bacillus subtilis. bioRxiv 2021.01.13.426625.
740 32. Calamita HG, Doyle RJ. 2002. Regulation of autolysins in teichuronic acid-
741 containing Bacillus subtilis cells. Mol Microbiol 44:601–606.
742 33. Atilano ML, Pereira PM, Yates J, Reed P, Veiga H, Pinho MG, Filipe SR. 2010.
743 Teichoic acids are temporal and spatial regulators of peptidoglycan cross-linking
744 in Staphylococcus aureus. ProcNatlAcadSciUSA 107:18991–18996.
745 34. Yamamoto H, Miyake Y, Hisaoka M, Kurosawa SI, Sekiguchi J. 2008. The major

and minor wall teichoic acids prevent the sidewall localization of vegetative DL-endopeptidase LytF in Bacillus subtilis. Mol Microbiol 70:297–310.

35. Reith J, Mayer C. 2011. Peptidoglycan turnover and recycling in Gram-Positive bacteria. Appl Microbiol Biotechnol 92:1–11.

36. Vitkovic L, Cheung HY, Freese E. 1984. Absence of correlation between rates of cell wall turnover and autolysis shown by Bacillus subtilis mutants. J Bacteriol 157:318–320.

37. Welsh MA, Taguchi A, Schaefer K, Van Tyne D, Lebreton F, Gilmore MS, Kahne D, Walker S. 2017. Identification of a Functionally Unique Family of Penicillin-Binding Proteins. J Am Chem Soc 139:17727–17730.

38. Leclerc D, Asselin A. 1989. Detection of bacterial cell wall hydrolases after denaturing polyacrylamide gel electrophoresis. Can J Microbiol 35:749–753.

39. Ursell T, Lee TK, Shiomi D, Shi H, Tropini C, Monds RD, Colavin A, Billings G, Bhaya-Grossman I, Broxton M, Huang BE, Niki H, Huang KC. 2017. Rapid, precise quantification of bacterial cellular dimensions across a genomic-scale knockout library. BMC Biol 15:1–15.

40. Dion MF, Kapoor M, Sun Y, Wilson S, Ryan J, Vigouroux A, van Teeffelen S, Oldenbourg R, Garner EC. 2019. Bacillus subtilis cell diameter is determined by the opposing actions of two distinct cell wall synthetic systems. Nat Microbiol https://doi.org/10.1038/s41564-019-0439-0.

41. Van Valen DA, Kudo T, Lane KM, Macklin DN, Quach NT, DeFelice MM, Maayan I, Tanouchi Y, Ashley EA, Covert MW. 2016. Deep Learning Automates the Quantitative Analysis of Individual Cells in Live-Cell Imaging Experiments. PLoS

769 Comput Biol 12:1–24.
770 42. Foster SJ. 1991. Cloning, expression, sequence analysis and biochemical
771 characterization of an autolytic amidase of Bacillus subtilis 168 trpC2. J Gen
772 Microbiol 137:1987–98.
773 43. Foster SJ. 1993. Analysis of Bacillus subtilis 168 prophage-associated lytic
774 enzymes; Identification and characterization of CWLA-related prophage proteins.
775 J Gen Microbiol 139:3177–3184.
776 44. Kuroda A, Sekiguchi J. 1990. Cloning, sequencing and genetic mapping of a
777 Bacillus subtilis cell wall hydrolase gene. J Gen Microbiol 136:2209–2216.
778 45. Nugroho FA, Yamamoto H, Kobayashi Y, Sekiguchi J. 1999. Characterization of a
779 new sigma-K-dependent peptidoglycan hydrolase gene that plays a role in
780 Bacillus subtilis mother cell lysis. J Bacteriol 181:6230–6237.
781 46. Longchamp PF, Mauel C, Karamata D. 1994. Lytic enzymes associated with
782 defective prophages of Bacillus subtilis: Sequencing and characterization of the
783 region comprising the N-acetylmuramoyl-L-alanine amidase gene of prophage
784 PBSX. Microbiology 140:1855–1867.
785 47. Regamey A, Karamata D. 1998. The N-acetylmuramoyl-L-alanine amidase
786 encoded by the Bacillus subtilis 168 prophage SPβ. Microbiology 144:885–893.
787 48. Kuroda A, Asami Y, Sekiguchi J. 1993. Molecular cloning of a sporulation-specific
788 cell wall hydrolase gene of Bacillus subtilis. J Bacteriol 175:6260–6268.
789 49. Smith TJ, Foster SJ. 1995. Characterization of the involvement of two
790 compensatory autolysins in mother cell lysis during sporulation of Bacillus subtilis
791 168. J Bacteriol 177:3855–3862.

792 50. Sekiguchi J, Akeo K, Yamamoto H, Khasanov FK, Alonso JC, Kuroda A. 1995.
793 Nucleotide sequence and regulation of a new putative cell wall hydrolase gene,
794 cwlD, which affects germination in Bacillus subtilis. J Bacteriol 177:5582–5589.
795 51. Popham DL, Helin J, Costello CE, Setlow P. 1996. Muramic lactam in
796 peptidoglycan of Bacillus subtilis spores is required for spore outgrowth but not for
797 spore dehydration or heat resistance. Proc Natl Acad Sci U S A 93:15405–15410.
798 52. Margot P, Karamata D. 1992. Identification of the structural genes for N-
799 acetylmuramoyl-L-alanine amidase and its modifier in Bacillus subtilis 168:
800 inactivation of these genes by insertional mutagenesis has no effect on growth or
801 cell separation. Mol Gen Genet 232:359–66.
802 53. Lazarevic V, Margot P, Soldo B, Karamata D. 1992. Sequencing and analysis of
803 the Bacillus subtilis lytRABC divergon: a regulatory unit encompassing the
804 structural genes of the N-acetylmuramoyl-L-alanine amidase and its modifier. J
805 Gen Microbiol 138:1949–1961.
806 54. Kuroda A, Sekiguchi J. 1991. Molecular cloning and sequencing of a major
807 Bacillus subtilis autolysin gene. J Bacteriol 173:7304–7312.
808 55. Fischer KE, Bremer E. 2012. Activity of the osmotically regulated yqiHIK promoter
809 from bacillus subtilis is controlled at a distance. J Bacteriol 194:5197–5208.
810 56. Morlot C, Uehara T, Marquis KA, Bernhardt TG, Rudner DZ. 2010. A highly
811 coordinated cell wall degradation machine governs spore morphogenesis in
812 Bacillus subtilis. Genes Dev 24:411–422.
813 57. Chastanet A, Losick R. 2007. Engulfment during sporulation in Bacillus subtilis is
814 governed by a multi-protein complex containing tandemly acting autolysins. Mol

Microbiol 64:139–152.

58. Palomino MM, Sanchez-Rivas C, Ruzal SM. 2009. High salt stress in Bacillus subtilis: involvement of PBP4* as a peptidoglycan hydrolase. Res Microbiol 160:117–124.

59. Lambert EA, Sherry N, Popham DL. 2012. In vitro and in vivo analyses of the Bacillus anthracis spore cortex lytic protein SleL. Microbiology 158:1359–1368.

60. Lambert EA, Popham DL. 2008. The Bacillus anthracis SleL (YaaH) protein is an N-Acetylglucosaminidase involved in spore cortex depolymerization. J Bacteriol 190:7601–7607.

61. Üstok FI, Chirgadze DY, Christie G. 2015. Structural and functional analysis of SleL, a peptidoglycan lysin involved in germination of Bacillus spores. Proteins Struct Funct Bioinforma 83:1787–1799.

62. Margot P, Mauël C, Karamata D. 1994. The gene of the N-acetylglucosaminidase, a Bacillus subtilis 168 cell wall hydrolase not involved in vegetative cell autolysis. Mol Microbiol 12:535–545.

63. Rashid MH, Mori M, Sekiguchi J. 1995. Glucosaminidase of Bacillus subtilis: Cloning, regulation, primary structure and biochemical characterization. Microbiology 141:2391–2404.

64. Horsburgh GJ, Atrih A, Williamson MP, Foster SJ. 2003. LytG of Bacillus subtilis is a novel peptidoglycan hydrolase: The major active glucosaminidase. Biochemistry 42:257–264.

65. Quay DHX, Cole AR, Cryar A, Thalassinos K, Williams MA, Bhakta S, Keep NH. 2015. Structure of the stationary phase survival protein YuiC from B.subtilis

838 Crystallography. BMC Struct Biol 15:1–14.
839 66. Ishikawa S, Yamane K, Sekiguchi J. 1998. Regulation and characterization of a
840 newly deduced cell wall hydrolase gene (cwlJ) which affects germination of
841 Bacillus subtilis spores. J Bacteriol 180:1375–1380.
842 67. Moriyama R, Fukuoka H, Miyata S, Kudoh S, Hattori A, Kozuka S, Yasuda Y,
843 Tochikubo K, Makino S. 1999. Expression of a germination-specific amidase,
844 sleB, of bacilli in the forespore compartment of sporulating cells and its
845 localization on the exterior side of the cortex in dormant spores. J Bacteriol
846 181:2373–2378.
847 68. Boland FM, Atrih A, Chirakkal H, Foster SJ, Moir A. 2000. Complete spore-cortex
848 hydrolysis during germination of Bacillus subtilis 168 requires SleB and YpeB.
849 Microbiology 146:57–64.
850 69. Heffron JD, Orsburn B, Popham DL. 2009. Roles of Germination-Specific Lytic
851 Enzymes CwlJ and SleB in Bacillus anthracis. J Bacteriol 191:2237–2247.
852 70. Sudiarta IP, Fukushima T, Sekiguchi J. 2010. Bacillus subtilis CwlQ (previous
853 YjbJ) is a bifunctional enzyme exhibiting muramidase and soluble-lytic
854 transglycosylase activities. Biochem Biophys Res Commun 398:606–612.
855 71. Beachy EH, Keck W, de Pedro MA, Schwarz U. 1981. Exoenzymatic Activity of
856 Transglycosylase Isolated from Escherichia coli. Eur J Biochem 116:355–358.
857 72. Sudiarta IP, Fukushima T, Sekiguchi J. 2010. Bacillus subtilis CwlP of the Sp-β
858 prophage has two novel peptidoglycan hydrolase domains, muramidase and
859 cross-linkage digesting DD-endopeptidase. J Biol Chem 285:41232–41243.
860 73. Fukushima T, Kitajima T, Yamaguchi H, Ouyang Q, Furuhata K, Yamamoto H,

Shida T, Sekiguchi J. 2008. Identification and characterization of novel cell wall hydrolase CwlT: A two-domain autolysin exhibiting N-acetylmuramidase and DL-endopeptidase activities. J Biol Chem 283:11117–11125.

74. Jorgenson MA, Chen Y, Yahashiri A, Popham DL, Weiss DS. 2014. The bacterial septal ring protein RlpA is a lytic transglycosylase that contributes to rod shape and daughter cell separation in Pseudomonas aeruginosa. Mol Microbiol 93:113–128.

75. Kerff F, Amoroso A, Herman R, Sauvage E, Petrella S, Filée P, Charlier P, Joris B, Tabuchi A, Nikolaidis N, Cosgrove DJ. 2008. Crystal structure and activity of Bacillus subtilis YoaJ (EXLX1), a bacterial expansin that promotes root colonization. Proc Natl Acad Sci U S A 105:16876–16881.

76. Abanes-De Mello A, Sun YL, Aung S, Pogliano K. 2002. A cytoskeleton-like role for the bacterial cell wall during engulfment of the Bacillus subtilis forespore. Genes Dev 16:3253–3264.

77. Kuroda A, Rashid MH, Sekiguchi J. 1992. Molecular cloning and sequencing of the upstream region of the major Bacillus subtilis autolysin gene: a modifier protein exhibiting sequence homology to the major autolysin and the spoIID product. J Gen Microbiol 138:1067–1076.

78. Kuroda A, Sekiguchi J. 1992. Characterization of the Bacillus subtilis CwbA protein which stimulates cell wall lytic amidases. FEMS Microbiol Lett 95:109–113.

79. Margot P, Wahlen M, Gholamhuseinian A, Piggot P, Karamata D. 1998. The lytE gene of Bacillus subtilis 168 encodes a cell wall hydrolase. J Bacteriol 180:749–

752.

80. Ishikawa S, Hara Y, Ohnishi R, Sekiguchi J. 1998. Regulation of a new cell wall hydrolase gene, cwlF, which affects cell separation in Bacillus subtilis. J Bacteriol 180:2549–2555.

81. Margot P, Pagni M, Karamata D. 1999. Bacillus subtilis 168 gene lytF encodes a 7-D- muropeptidase expressed by the alternative vegetative sigma factor , cD. Microbiology 145:57–65.

82. Ohnishi R, Ishikawa S, Sekiguchi J. 1999. Peptidoglycan hydrolase LytF plays a role in cell separation with CwlF during vegetative growth of Bacillus subtilis. J Bacteriol 181:3178–3184.

83. Suzuki T, Tahara Y. 2003. Characterization of the Bacillus subtilis ywtD gene, whose product is involved in γ-polyglutamic acid degradation. J Bacteriol 185:2379–2382.

84. Schmidt DMZ, Hubbard BK, Gerlt JA. 2001. Evolution of enzymatic activities in the enolase superfamily: Functional assignment of unknown proteins in bacillus subtilis and Escherichia coli as L-Ala-D/L-Glu epimerases. Biochemistry 40:15707–15715.

85. Hourdou ML, Guinand M, Vacheron MJ, Michel G, Denoroy L, Duez C, Englebert S, Joris B, Weber G, Ghuysen JM. 1993. Characterization of the sporulation-related γ-D-glutamyl-(L)mesodiaminopimelic-acid-hydrolysing peptidase I of Bacillus sphaericus NCTC 9602 as a member of the metallo(zinc) carboxypeptidase A family: Modular design of the protein. Biochem J 292:563–570.

907 86. Fukushima T, Yao Y, Kitajima T, Yamamoto H, Sekiguchi J. 2007.
908 Characterization of new L,D-endopeptidase gene product CwlK (previous YcdD)
909 that hydrolyzes peptidoglycan in Bacillus subtilis. Mol Genet Genomics 278:371–
910 383.
911 87. Horsburgh GJ, Atrih A, Foster SJ. 2003. Characterization of LytH, a
912 differentiation-associated peptidoglycan hydrolase of Bacillus subtilis involved in
913 endospore cortex maturation. J Bacteriol 185:3813–3820.
914